In situ Elastic Strain Measurements-Diffraction and Spectroscopy

R. Spolenak, Wolfgang Ludwig, Jean-Yves Buffiere, J. Michler

In-situ elastic strain measurements – diffraction and spectroscopy

R. Spolenak, W. Ludwig, J. Y. Buffiere, J. Michler

1 Introduction

X-ray diffraction is a common tool to determine order in materials. Based on Bragg's equation, the average distance of nearest neighbors of atoms or molecules can be determined. In crystalline materials, a high degree of ordering results in very sharp diffraction peaks. The sharpness of this peaks allows for a highly accurate determination of atomic spacing and consequently of elastic strains (deviations from the equilibrium lattice spacing) and the calculation of stress tensors. In addition, any deviation of perfect periodicity, which exhibits itself in the broadening and asymmetry of diffraction peaks, renders information of the imperfections in materials, namely their microstructure. These imperfections range from grain-boundaries, stacking faults, implantation defects over interfaces and dislocations to the degree of disorder in amorphous materials. The following will demonstrate how, both aspects of X-ray diffraction can be combined with in-situ tests to gain insight into the mechanisms of mechanical behavior of materials. In addition, a complementary technique of Raman spectroscopy is addressed, where similar concepts apply. X-ray diffraction concepts in principal also apply to electron and neutron diffraction. The latter are, however, omitted here for the sake of brevity.

2 X-ray diffraction (2000 words)

2.1 Basic principles of X-ray diffraction

The basis for X-ray diffraction is Bragg's equation:

$$n\lambda = 2d\sin\theta \tag{1.1}$$

Where d is the lattice spacing, θ the diffraction angle in a classical diffraction set-up and λ the wavelength of X-rays. Differentiation of Bragg's equation yields

$$\Delta\theta = -\frac{\Delta d}{d}\tan\theta \tag{1.2}$$

Which shows that measurements at higher diffraction angle (usually high order diffraction lines), are more accurate. In defect free polycrystals, grain size can be determined by Scherrer's formula:

$$\Delta 2\theta^\circ = \frac{\lambda}{D\cos\theta}\frac{180}{\pi} \tag{1.3}$$

Where $\Delta 2\theta$ is the full width at half maximum of the diffraction peak in addition to the instrumental broadening and D is the grain size. If dislocations are also present the shape of peaks and its change with the order of reflection needs to be taken into account. This is elegantly done by obtaining the

Fourier coefficients of each peak in the classical Warren-Averbach analysis [1]. The latter technique, however, requires the possibility of measuring high order peaks, which is not always possible in an in-situ set-up.

2.2 Non local measurements

Due to the spot size of laboratory X-ray sources, which is usually much bigger than the grain size in typical polycrystalline materials, the diffracted signal originates from a polycrystalline ensemble and powder-like spectra are acquired. The difficulty in the determination of elastic strains is that the measured lattice distance needs to be related to the equilibrium lattice spacing. Accurate elastic strain measurements require the equilibrium lattice parameter to be determined experimentally. The usual pathway is explained in the following.

2.2.1 Sin²ψ – technique

The angle ψ is defined as the angle between the normal of the diffracting planes and the surface normal of the material investigated (see Fig. 1). Surfaces are stress free in their normal direction and the material underneath can be stressed in tension or compression. Consequently, if the elastic strain is probed at different angles to the surface normal (different angles ψ), it has to go through zero at a specific angle. Consequently, the reference is incorporated in the measurement. For an equibiaxial stress state in an elastically isotropic material stress and elastic strain can be derived from the following equation:

$$\frac{d_\psi - d_0}{d_0} = \frac{1+\nu}{E}\sigma_b \sin^2\psi - \frac{2\nu}{E}\sigma_b \tag{1.4}$$

The angle for zero strain consequently depends on the elastic properties of the material investigated. More complex stress states and elastically anisotropic materials are treated in an excellent book by Noyan and Cohen [2].

Several examples of in-situ measurements can be found in [3-4] and [5]. However, the measurement time required is significant. This can be overcome by using synchrotron sources and/or using the following technique.

2.2.2 Sin²φ – technique

The $\sin^2\varphi$ – technique as described in Wanner *et al.* [6] is a relative technique and thus requires the determination of the residual stress state at the beginning of the experiment. This can be accomplished by the $\sin^2\psi$ – technique. It is based on measuring the diameter of Debye-Scherrer rings by an area or two crossed linear detectors. If a strain is applied in the sample plane, the Debye-Scherrer rings are distorted into ellipses, whose ellipticity can be used to quantify the elastic strain. No change in diffraction geometry is required during an in-situ experiment. If a textured material is investigated the X-ray source needs to be tunable and thus experiments are limited to synchrotron sources [7]. Details of the geometry can be found in Fig. 1.

Recently, this method has been applied extensively to the investigation of scaling in yield strength of thin films [8-9] and arrays of metal nanowires [10]. Stress-strain curves of metallic structures with features sizes down to 20 nm could be investigated, shedding new light on the materials deformation mechanisms. Specifically, the significant temperature and strain-rate dependence of nanocrystalline

Au nanostructures is worth mentioning. Strain-rate experiments by X-ray diffraction can only be achieved by short measurement times (e.g. 5 s per strain step) offered by the $\sin^2\varphi$– technique.

An interesting example of the application of several in-situ techniques, namely, the $\sin^2\varphi$– technique, scanning electron microscopy and optical microscopy can be seen in Fig. 2. Here, the fracture and delamination behavior of thin brittle metal films (i.e. Ta) are investigated [11]. The onset of cracking can be determined as a stress drop in the stress-strain curve in tensile direction, a change in slope in the stress-strain curve in transverse direction and the direct observation of first cracks. Cracking results in the build-up of compressive stress in normal direction, due to the relaxation of tensile stresses and consequently reduced Poisson contraction compared to the substrate. This in turn leads to thin film delamination until finally most of the strain is carried by the substrate. Such experiments are utilized to determine both the fracture toughness of the thin films and the energy release rate of interfacial cracks. Further insights into the deformation mechanisms can be gained by focusing X-rays and resolving elastic strains at a more local scale.

2.3 Local stress measurements in 2D

2.3.1 Monochromatic microdiffraction

When mapping of local stresses is required at a medium spatial resolution (a few tens of micrometers), monochromatic synchrotron X-rays can simply be restricted by slits to produce 2D maps of stress in transmission mode [12]. This is comparable to the $\sin^2\varphi$– technique , but allows for the mapping of elastic strain states. Furthermore, this kind of diffraction experiment can be efficiently combined with 3D tomographic imaging (see also below), to investigate the stress redistribution induced by the development of damage in a material under various experimental environments (applied load, temperature cycles). Such in-situ experiments were performed, for instance, at beamlines ID15, ID11 and ID19 of ESRF, on Ti/SiC_f metal matrix composites [13-14]. For this last material, by combining 3D images of cracks in the SiC fibers and the diffraction profile recorded along the same fibers and in the neighboring matrix, it was possible to show the effect of elastic strain partitioning from the fibers to the matrix and to evaluate the interfacial shear strength along the fibers, a key parameter for the modeling of the mechanical behavior of this kind of high performance material.

When higher spatial resolution is needed, monochromatic X-rays can most easily be focused by Fresnel zone plates or refractive X-ray optics, the latter being less efficient at higher X-ray energies. In most cases the X-ray beam then becomes smaller than the grain size. Consequently, single crystal diffraction has to be applied and sample tilting is required. Measurements at a length scale of around one micrometer and less are however problematic due to the sphere of confusion of currently available diffractometers. Consequently, successful in-situ work has been limited to highly textured polycrystalline materials [15-17] for monitoring the stress and composition evolution during electromigration, single crystals by microdiffraction topography [18] for indirect measurement of stress in patterned thin films and small angle X-ray diffraction [19] for monitoring the structure evolution in spider silk fabrication. All these experiments can be performed without sample tilt during the in-situ experiment.

2.3.2 Laue microdiffraction

Laue microdiffraction [20] solves the "tilt" problem described above for randomly oriented polycrystalline specimen. In this technique a white or pink X-ray beam is focused by achromatic Kirkpatrick-Baez mirrors to spots down to 500 nm diameter, which in turn renders this technique applicable to grain sizes of minimal 200 nm. The locally single crystalline sample now acts as an analyzer for the polychromatic beam resulting in a typical Laue pattern, where in contrast to standard diffraction techniques the wavelength rather than the diffraction angle is altered. A combination of well calibrated area detectors and a reference pattern allows for the determination of the complete deviatoric strain tensor in a resolution of 10^{-4} [21]. The lattice parameter can in principle be determined by using a monochromator and scanning the wavelength or by analyzing the wavelength of the diffracted beam. The first approach is more accurate, but has not yet reached the accuracy levels of the deviatoric strain determination. In addition to elastic strain also phases and defect densities can be determined. Peak broadening in this technique is a direct measure of geometrically necessary dislocations or small-angle grain boundaries [22], similarly but more accurately than electron backscatter diffraction (EBSD). Classical peak broadening would be reflected in a broadening in energy space.

Pioneered by the Advanced Photon Source (APS) at Argonne National Laboratory, several Laue microdiffraction beamlines have been set-up world wide, e.g. at the Advanced Light Source (ALS), Lawrence Berkeley Labs, the European Synchrotron Radiation Facility (ESRF), the Swiss Light Source (SLS) and the Canadian Light Source (CLS). Broad beam in-situ Laue diffraction has been demonstrated at the Karlsruhe synchrotron (ANKA) [23]. Most in-situ experiments have been carried out at the ALS as there the first dedicated beamline was built, of which two examples will be described in the following.

The easiest way of performing a mechanical in-situ experiment involving thin films is depositing them on a substrate of strongly different coefficient of thermal expansion with regards to the thin film. Stresses can then be induced by thermal cycling of the sample. Laue microdiffraction in such experiments revealed strong variations of stress from grain to grain (ca. 100 MPa) and significant stress gradients within a grain [24]. Recently, a novel mechanism for grain rotation, namely a combination of dislocation and disclination motion has been elucidated [25].

The directional transport of mass due to an electric current (electromigration) poses a reliability concern for microelectronic devices. In-situ Laue microdiffraction was able to show that hillocks at the anode end of conductor lines are formed by dislocation climb [26-28].

2.4 3D stress measurements

2.4.1 Laue microdiffraction

The concept of Laue microdiffraction can be extended from 2D to 3D by selective absorption of the diffracted beams. This can be achieved by scanning a highly absorbing wire (knife edge) over the sample surface in a 45°-diffraction geometry [29]. This technique was used to study the deformation of copper underneath a nanoindent [30], however, the timescale for measurement is prohibitively long to allow for in-situ observations.

2.4.2 Three Dimensional Diffraction Microscopy (3DXRD)

3D elastic strain measurement techniques based on monochromatic X-ray beams can be subdivided into macroscopic (multi grain average) and microscopic (individual grain) approaches, similarly to the 2D approaches.

In the first case the sampled 3D volume element contains a large number of grains giving rise to diffraction into well defined directions, described by cones. The analysis of the position and intensity distribution on the ring-like diffraction patterns observed on a two-dimensional detector for several sample orientations gives access to components of the elastic strain state in the illuminated volume element. The localization of the diffracting volume element in three-dimensions can be achieved by insertion of pinholes and/or beam defining slits (e.g. conical slits for observation of simultaneous observation of entire diffraction cones).

In the second case only a limited number of grains are contained in the illuminated sample volume. One may now observe and analyze the position of individual diffraction spots on the detector. The latter methodology is termed three-dimensional X-ray diffraction microscopy (3DXRD) and has been reviewed in the book by Poulsen [31]. Note that in this condition the sample needs to be rotated over an extended angular range in order to record several reflections from each of the grains. With a suited combination of detector resolution and distance, the position, size, average orientation and the full elastic strain tensor for each of the grains can be determined from such a set of diffraction images [32]. The timescale for this kind of grain resolved strain measurement is of order of a few minutes using synchrotron radiation.

Placing an additional high resolution detector system closely behind the sample one can analyze the 2D intensity distribution inside the diffraction spots. The latter can be assimilated as two-dimensional projections of the grain volumes and the use of tomographic or stochastic reconstruction approaches permit to reconstruct the three-dimensional grain shapes (see [31]).

The use of advanced data analysis routines permits extraction of local lattice orientation *inside* individual grains and has been demonstrated recently for layer like (1D) illumination mode [33]. It can be speculated that further refinement of the methodology will eventually give access to the local deformation tensor (orientation and elastic strain) at the sub-grain level. The time scale for this kind of measurements depends on the dimensions of the sampled volume and varies from a few minutes to several hours for scanning a two-dimensional section and a three-dimensional sample volume, respectively.

2.4.3 3D digital volume correlation and 3D particle tracking techniques

The presence of elastic strain in a material can be detected by measuring variations of the lattice parameter, as explained above. The total strain, on the other hand, can also be assessed, in principle, by measuring the displacement of elements of the microstructure between a reference and a deformed volume. Two different methods, called particle tracking (PT) and digital volume correlation (DVC) can be used. While the first one evaluates the displacements of microstructural features through the movement of their centre of mass, the second one uses correlation techniques to match the two volumes. Although the development of digital image correlation dates back to the eighties [34], its application to 3D tomographic images is much more recent (see for example [35] for a list). Both PT and DVC require the presence of markers within the images. Two different strategies have

been employed so far. One is to introduce artificially those markers in the studied material [36-37], the other one is to directly use the material microstructure [35, 38-41]. The first method can in principle be applied to a variety of materials, provided a suitable technique for distributing homogeneously the markers is found. However, the question of how much the presence of those features affect the deformation process remains an issue. From that point of view, natural markers appear more attractive, but the number of materials presenting a relevant microstructure is restricted. So far, the deformation of quite different «natural» materials has been studied: Al alloys, cast iron, trabecular bone, polystyrene foam, stone wool and wood to name a few.

Both PT and DVC provide displacements at a sub voxel scale. In the case of DVC the displacement uncertainty appears to be higher than that reported for 2D images [35], probably because of the noise introduced in the images during the reconstruction process. This is likely to be also the case for PT but to the author's knowledge , a comparison between 2D and 3D accuracy has not been reported so far for PT. Values of uncertainties ranging between 10^{-1} to 10^{-2} voxels have been reported, depending on the material and the method used [35]. In the case of DVC, the level of uncertainty can be reduced by using larger elements for correlation. However this is done at the expense of the spatial accuracy of the measurement. If very short range variations of the displacement field are to be captured then a lower element size should be used resulting in a higher uncertainty (and vice versa). For PT the accuracy with which the displacement field is captured is dictated by the typical distance between markers.

One important application of kinematic measurements in the bulk of a material is the evaluation of the displacement field at the tip of a crack. This technique then gives a direct evaluation of the crack driving force via the extraction of the mixed mode stress intensity factor as explained for example by Rannou *et al.* [42]. This has been done in Al alloys using the tracking technique [40] and also in cast iron by using DVC [35]. Fig. 3 shows an example of the results that can be obtained with DVC regarding the quantification of 3D opening of a fatigue crack under load.

2.4.4 Merging the concepts of Diffraction and Imaging

For some classes of polycrystalline materials, the concepts of 3D X-ray diffraction microscopy and tomographic imaging can be merged: the combined methodology, termed X-ray diffraction contrast tomography (DCT), provides simultaneous access to the three-dimensional distribution of the X-ray attenuation coefficient as well as to the grain microstructure described in terms of shape, orientation and elastic strain tensors for each grain [43]. Similar to outlined 3DXRD methodology, the three-dimensional reconstruction of grain shapes is achieved via analysis of the *shape* of the diffraction spots, observed on a high resolution X-ray imaging detector positioned a few millimeters down-stream the sample. Efforts are underway to combine the concepts of DVC and DCT for total strain evaluation during tensile deformation studies.

3 Raman spectroscopy

3.1 Basic principles

Fig. 4a shows the experimental set-up of a typical micro-Raman instrument [44-45]. Light from the laser is focused onto a sample of interest, such as a micropillar under load, using microscope objectives and sample micropositioners. The scattered light is collected and directed into a

premonochromator and a spectrometer for detection by a Charge Coupled Device (CCD) system. If a 100x objective (numerical aperture of 0.9) is used, a probing spot with a diameter of 500 to 300 nm can be obtained, depending on the optical system and on the wavelength of light. A further reduction of spot size can conventionally only be achieved by the use of wavelength in the UV range or the application of oil immersion objectives. The probe depth ranges from a few nm to mm depending on the optical properties of the materials, and can be limited to the submicron range via a confocal setup.

Raman scattering arises from an inelastic interaction between photons (light of the incident laser) and phonons (vibrations of the crystal lattice). Spectral analysis of the scattered light reveals distinct peaks that are related to particular optical phonon modes (zone centre optical phonons, i.e. k=0 selection rule) in the crystal, providing a unique fingerprint of the latter. Spectra from amorphous materials exhibit broad bands which can be rationalized by considering all possible phonon modes in a crystal. Raman-active materials, in this sense, are many semiconductor and ceramic materials. Raman active samples are also many types of molecules, nanotubes and polymers due to molecular vibrations, where different selection rules apply [46]. The difference between the frequency of the scattered and the incident light is called the Raman shift, expressed in wavenumbers (cm^{-1}). The number of Raman peaks that can be observed depends on the crystal symmetry, the polarization directions of the incident and detected light and the propagation directions of the incident and detected beams with respect to the crystal axes. For instance silicon in the stable phase at ambient conditions, e.g. the diamond structure, exhibits a single peak around 520 cm^{-1} (one-phonon mode) and additional weak two-phonon mode peaks. During an unloading from high hydrostatic pressure - for instance during unloading of a nanoindentation experiment - a sequence of other crystal structures and amorphous silicon can form below the contact area each exhibiting a characteristic number of peaks at different wavenumbers [46]. Finite size of crystalline grains in the nanometer range significantly alters the Raman spectrum; selection rules derived from the assumption of infinite crystals relax, leading to an asymmetric peak broadening in most cases, as phonons with lower or higher frequencies participate in the scattering process. Crystal defects, such as dislocations formed during plastic deformation or interstitials formed during implantation, generate microstrains resulting in a symmetric peak broading.

Elastic strain changes the frequency of lattice vibrations and, therefore, will shift the Raman peaks. Peak shifts vary linear with stress components and the related coefficients are well documented for many materials [47]. Some prior knowledge of the stress distribution is, however, required, since in many cases the stress tensor leads to shifts and shape changes of a single peak only. In many cases simple uniaxial or biaxial stress states are studied.

If Raman spectroscopy is combined with a micromechanical testing setup, phase transformations or changes in the microstructure during loading would alter the spectrum or peak shapes, respectively. The stress field can be probed with one micrometer resolution through monitoring the peak positions. When the nature of stress state is known through the loading conditions, the observed peak shifts can be converted easily into local stress values, i.e. the Raman spectrum serves as a microscopic elastic strain gage on the sample. A frequency change of ~0.02 cm^{-1} can be detected using state-of-the-art equipment, which translates to a stress resolution of roughly 10 MPa for most materials. An in-situ microcompression experiment on silicon <001> oriented pillars is shown

schematically in Fig. 4b [48]. During the uniaxial compression, good agreement between the stress measured by the micro-indenter load cell and the stress deduced by the Raman peak shift in the elastic region was found. Small shoulders at lower peak frequencies are evidence of crack propagation and corresponding stress relaxation prior to brittle fracture of the silicon pillars. In-situ Raman micro-compression experiments on <001> GaAs pillars of similar size demonstrated the capability of this technique in determining the onset of plastic deformation. While the Raman peak undergoes monotonically positive shifts linearly proportional to the increase in elastic strain, the onset of plasticity and the corresponding load drop is seen as a sudden negative shift. During plastic deformation the peak is seen to broaden due to increased dislocation density and inhomogeneous plastic deformation localized with well defined glide bands emanating from the contact edge between flat punch and micro-pillar [49].

3.2 Resolution beyond the diffraction limit

Elastic strain is very important in the semiconductor industry because it boosts the speed and reduces the power consumption of electronic devices. Focusing the exciting laser on the sample surface gives, at best, probing spots in the order of ~1 μm. Developments in near-field Raman spectroscopy have produced novel measurement techniques that allow nanoscale lateral resolution. One approach is to guide laser light onto a tip with a very small aperture of diameter 50-200 nm. The tip is held at a distance of ~10 nm above the sample (near-field scanning optical microscopy – NSOM). NSOM has been used to analyse elastic strain in crystalline samples [50]. The spatial resolution is restricted to about 150 nm due to significant power losses in small apertures. An alternative approach to circumvent the optical diffraction barrier was proposed by Wessel [51] based on a discovery by Fleischmann [52]. The Raman scattering cross-section is enhanced by many orders of magnitude by placing a metal in contact with the sample surface [53]. This so-called surface-enhanced Raman scattering (SERS) effect is mainly due to an electromagnetic field-enhancement occurring near surface irregularities through the excitation of localized surface plasmons by light [54-55]. By replacing the metal grains with a metallic nanometer sized tip (see Fig. 4c), the enhancement can be localized [56-58]. Provided that the scattering comes predominantly from the contact area, a resolution of several tens of nanometers can be achieved. The resulting tip-enhanced Raman spectroscopy (TERS) is capable of measuring Raman spectra with high spatial resolution, effectively overcoming the diffraction limit. A successful TERS experiment depends heavily on the ability to fabricate tips of a definite metal with the appropriate shape and size, which is still a challenging process [59-61]. The ultimate goal would be to try to integrate the TERS experiment, i.e. nanoscale mapping capabilities, into an in-situ micromechanical testing setup like a tensile or compression test on a microscopic sample.

4 Stress and microstructure

An addition to the determination of stress during an in-situ experiment is also the monitoring of microstructural changes. Peak broadening was found to be reversible in nanocrystalline Al below a grain size of 80 nm indicating the absence of dislocation storage mechanisms [5]. Maass *et al.* [62-63] were able to correlate the peak broadening and peak shift in in-situ Laue microdiffraction compression experiments to the glide systems present. Consequently, in the metal pillar dimension

the mechanical behavior of small volumes is mostly determined by the microstructure rather than the absolute value of pillar dimension.

Complementary application of transmission electron microscopy and micro-Raman spectroscopy on the same sample area allows for direct imaging of the residual stress field of lattice defects like dislocations and disclinations [55] and of crystal structures formed due to phase transformations during a nanoindentation experiment [64-65].

Future challenges of in-situ elastic strain measurements will involve:

- Improved spatial resolution: Focusing of probes down to the ten nanometer length scale will also pose challenges for spatial stability as measurement time will increase.
- Quantification of defect structures: Direct correlation between atomistic modeling and complementary experimental techniques is required to quantify character and magnitude of defects and their changes during deformation.
- Reduction in measurement time for dynamical experiments: Here a compromise will have to be found between time scale and spatial resolution.
- Solving space constraints of in-situ experimental set-ups: A quantitative analysis of defect structures requires large scattering angles or sample tilts. This would require a miniaturized design of in-situ test equipment.
- The interpretation of coherency effects in small scale diffraction: see [66].

5 Acknowledgments

JM acknowledges Pierre Brodard, EMPA for help with the figures. RS acknowledges Patric Gruber and Stephan Frank for help with the figures.

6 References

1. Warren, B.E. and B.L. Averbach, *The Separation of Cold Work Distortion and Particle Size Broadening in X-Ray Patterns.* Physical Review, 1952. **86**(4): p. 656-656.
2. Noyan, I.C. and J.B. Cohen, *Residual Stress*. 1987, New York: Springer.
3. Hommel, M. and O. Kraft, *Deformation behavior of thin copper films on deformable substrates.* Acta Materialia, 2001. **49**(19): p. 3935-3947.
4. Kraft, O., M. Hommel, and E. Arzt, *X-ray diffraction as a tool to study the mechanical behaviour of thin films.* Materials Science and Engineering a-Structural Materials Properties Microstructure and Processing, 2000. **288**(2): p. 209-216.
5. Gianola, D.S., S. Van Petegem, M. Legros, S. Brandstetter, H. Van Swygenhoven, and K.J. Hemker, *Stress-assisted discontinuous grain growth and its effect on the deformation behavior of nanocrystalline aluminum thin films.* Acta Materialia, 2006. **54**(8): p. 2253-2263.
6. Wanner, A. and D.C. Dunand, *Synchrotron x-ray study of elastic phase strains in the bulk of an externally loaded Cu/Mo composite.* Applications of Synchrotron Radiation Techniques to Materials Science V, 2000. **590**: p. 157-162

7. Bohm, J., P. Gruber, R. Spolenak, A. Stierle, A. Wanner, and E. Arzt, *Tensile testing of ultrathin polycrystalline films: A synchrotron-based technique.* Review of Scientific Instruments, 2004. **75**(4): p. 1110-1119.
8. Gruber, P.A., J. Bohm, F. Onuseit, A. Wanner, R. Spolenak, and E. Arzt, *Size effects on yield strength and strain hardening for ultra-thin Cu films with and without passivation: A study by synchrotron and bulge test techniques.* Acta Materialia, 2008. **56**(10): p. 2318-2335.
9. Gruber, P.A., S. Olliges, E. Arzt, and R. Spolenak, *Temperature dependence of mechanical properties in ultrathin Au films with and without passivation.* Journal of Materials Research, 2008. **23**(9): p. 2406-2419.
10. Olliges, S., P.A. Gruber, V. Auzelyte, Y. Ekinci, H.H. Solak, and R. Spolenak, *Tensile strength of gold nanointerconnects without the influence of strain gradients.* Acta Materialia, 2007. **55**(15): p. 5201-5210.
11. Frank, S., U.A. Handge, S. Olliges, and R. Spolenak, *The relationship between thin film fragmentation and buckle formation: Synchrotron-based in situ studies and two-dimensional stress analysis.* Acta Materialia, 2009. **57**(5): p. 1442-1453.
12. Korsunsky, A.M., K.E. Wells, and P.J. Withers, *Mapping two-dimensional state of strain using synchroton X-ray diffraction.* Scripta Materialia, 1998. **39**(12): p. 1705-1712.
13. Hung, Y.C., J.A. Bennett, F.A. Garcia-Pastor, M. Di Michlel, J.Y. Buffiere, T.J.A. Doel, P. Bowen, and P.J. Withers, *Fatigue crack growth and load redistribution in Ti/SiC composites observed in situ.* Acta Materialia, 2009. **57**(2): p. 590-599.
14. Sinclair, R., M. Preuss, E. Maire, J.Y. Buffiere, P. Bowen, and P.J. Withers, *The effect of fibre fractures in the bridging zone of fatigue cracked Ti-6Al-4V/SiC fibre composites.* Acta Materialia, 2004. **52**(6): p. 1423-1438.
15. Kao, H.K., G.S. Cargill, F. Giuliani, and C.K. Hu, *Relationship between copper concentration and stress during electromigration in an Al(0.25 at.% Cu) conductor line.* Journal of Applied Physics, 2003. **93**(5): p. 2516-2527.
16. Kao, H.K., G.S. Cargill, and C.K. Hu, *Electromigration of copper in Al(0.25 at. % Cu) conductor lines.* Journal of Applied Physics, 2001. **89**(5): p. 2588-2597.
17. Zhang, H., G.S. Cargill, Y. Ge, A.M. Maniatty, and W. Liu, *Strain evolution in Al conductor lines during electromigration.* Journal of Applied Physics, 2008. **104**(12): p. 123533.
18. Yan, H.F., C.E. Murray, and I.C. Noyan, *Mapping local strain in thin film/substrate systems using x-ray microdiffraction topography.* Applied Physics Letters, 2007. **90**(9): p. 091918.
19. Riekel, C., M. Muller, and F. Vollrath, *In situ X-ray diffraction during forced silking of spider silk.* Macromolecules, 1999. **32**(13): p. 4464-4466.
20. Ice, G.E., J.S. Chung, B.C. Larson, J.D. Budai, J.Z. Tischler, N. Tamura, and W. Lowe, *Design and performance of x-ray optics optimized for polycrystalline microdiffraction.* Synchrotron Radiation Instrumentation, 2000. **521**: p. 19-24
21. Tamura, N., R.S. Celestre, A.A. MacDowell, H.A. Padmore, R. Spolenak, B.C. Valek, N.M. Chang, A. Manceau, and J.R. Patel, *Submicron x-ray diffraction and its applications to problems in materials and environmental science.* Review of Scientific Instruments, 2002. **73**(3): p. 1369-1372.
22. Barabash, R.I., G.E. Ice, N. Tamura, B.C. Valek, J.C. Bravman, R. Spolenak, and J.R. Patel, *Quantitative analysis of dislocation arrangements induced by electromigration in a passivated Al (0.5 wt % Cu) interconnect.* Journal of Applied Physics, 2003. **93**(9): p. 5701-5706.
23. Gruber, P.A., C. Solenthaler, E. Arzt, and R. Spolenak, *Strong single-crystalline Au films tested by a new synchrotron technique.* Acta Materialia, 2008. **56**(8): p. 1876-1889.
24. Spolenak, R., et al., *Local plasticity of Al thin films as revealed by X-ray microdiffraction.* Physical Review Letters, 2003. **90**(9): p. 096102.

25. Nyilas, R.D., M. Kobas, and R. Spolenak, *Synchrotron X-ray microdiffraction reveals rotational plastic deformation mechanisms in polycrystalline thin films.* Acta Materialia, 2009. **57**(13): p. 3738-3753.
26. Budiman, A.S., W.D. Nix, N. Tamura, B.C. Valek, K. Gadre, J. Maiz, R. Spolenak, and J.R. Patel, *Crystal plasticity in Cu damascene interconnect lines undergoing electromigration as revealed by synchrotron x-ray microdiffraction.* Applied Physics Letters, 2006. **88**(23): p. 233515.
27. Valek, B.C., et al., *Electromigration-induced plastic deformation in passivated metal lines.* Applied Physics Letters, 2002. **81**(22): p. 4168-4170.
28. Valek, B.C., et al., *Early stage of plastic deformation in thin films undergoing electromigration.* Journal of Applied Physics, 2003. **94**(6): p. 3757-3761.
29. Larson, B.C., W. Yang, G.E. Ice, J.D. Budai, and J.Z. Tischler, *Three-dimensional X-ray structural microscopy with submicrometre resolution.* Nature, 2002. **415**(6874): p. 887-890.
30. Larson, B.C., W. Yang, J.Z. Tischler, G.E. Ice, J.D. Budai, W. Liu, and H. Weiland, *Micron-resolution 3-D measurement of local orientations near a grain-boundary in plane-strained aluminum using X-ray microbeams.* International Journal of Plasticity, 2004. **20**(3): p. 543-560.
31. Poulsen, H.F., *Three-Dimensional X-ray Diffraction Microscopy. Mapping Polycrystals and their Dynamics.* Springer Tracts in Modern Physics. 2004, Berlin: Springer.
32. Martins, R.V., L. Margulies, S. Schmidt, H.F. Poulsen, and T. Leffers, *Simultaneous measurement of the strain tensor of 10 individual grains embedded in an Al tensile sample.* Materials Science and Engineering a-Structural Materials Properties Microstructure and Processing, 2004. **387-89**: p. 84-88.
33. West, S.S., S. Schmidt, H.O. Sorensen, G. Winther, H.F. Poulsen, L. Margulies, C. Gundlach, and D.J. Jensen, *Direct non-destructive observation of bulk nucleation in 30% deformed aluminum.* Scripta Materialia, 2009. **61**(9): p. 875-878.
34. Sutton, M.A., H. Wolters, W.H. Peters, W.F. Ranson, and S.R. McNeill, *Determination of Displacements Using an Improved Digital Correlation Method.* Im. Vis. Comp., 1983. **1**(3): p. 133-139.
35. Limodin, N., J. Rethore, J.Y. Buffiere, A. Gravouil, F. Hild, and S. Roux, *Crack closure and stress intensity factor measurements in nodular graphite cast iron using three-dimensional correlation of laboratory X-ray microtomography images.* Acta Materialia, 2009. **57**(14): p. 4090-4101.
36. Haldrup, K., S.F. Nielsen, and J.A. Wert, *A general methodology for full-field plastic strain measurements using X-ray absorption tomography and internal markers.* Experimental Mechanics, 2008. **48**(2): p. 199-211.
37. Nielsen, S.F., H.F. Poulsen, F. Beckmann, C. Thorning, and J.A. Wert, *Measurements of plastic displacement gradient components in three dimensions using marker particles and synchrotron X-ray absorption microtomography.* Acta Materialia, 2003. **51**(8): p. 2407-2415.
38. Bay, B.K., T.S. Smith, D.P. Fyhrie, and M. Saad, *Digital volume correlation: Three-dimensional strain mapping using X-ray tomography.* Experimental Mechanics, 1999. **39**(3): p. 217-226.
39. Roux, S., F. Hild, P. Viot, and D. Bernard, *Three-dimensional image correlation from X-ray computed tomography of solid foam.* Composites Part a-Applied Science and Manufacturing, 2008. **39**(8): p. 1253-1265.
40. Toda, H., I. Sinclair, J.Y. Buffiere, E. Maire, K.H. Khor, P. Gregson, and T. Kobayashi, *A 3D measurement procedure for internal local crack driving forces via synchrotron X-ray microtomography.* Acta Materialia, 2004. **52**(5): p. 1305-1317.
41. Verhulp, E., B. van Rietbergen, and R. Huiskes, *A three-dimensional digital image correlation technique for strain measurements in microstructures.* Journal of Biomechanics, 2004. **37**(9): p. 1313-1320.

42. Rannou, J., N. Limodin, J. Rethore, A. Gravouil, M.-C. Baietto-Dubourg, J.Y. Buffiere, A. Combescure, F. Hild, and S. Roux, *Three dimensional experimental and numerical multiscale analysis of a fatigue crack* Comput. Methods Appl. Mech. Eng. , 2009. **doi:10.1016/j.cma.2009.09.013**
43. Ludwig, W., P. Reischig, A. King, M. Herbig, E.M. Lauridsen, G. Johnson, T.J. Marrow, and J.Y. Buffiere, *Three-dimensional grain mapping by x-ray diffraction contrast tomography and the use of Friedel pairs in diffraction data analysis.* Review of Scientific Instruments, 2009. **80**(3): p. 033905.
44. Grasselli, J.G. and B.J. Bulkin, *Analytical Raman Spectroscopy*. 1991: Wiley-Interscience.
45. Weber, W.H. and R. Merlin, *Raman Scattering in Materials Science*. Springer Series in Materials Science. 2000: Springer.
46. Gogotsi, Y., T. Miletich, M. Gardner, and M. Rosenberg, *Microindentation device for in situ study of pressure-induced phase transformations.* Rev. Sci. Instrum., 1999. **70**: p. 4612.
47. Anastassakis, E. and M. Cardona, *Phonons, strains, and pressure in semiconductors*, in *High Pressure in Semiconductor Physics II. Semiconductors and Semimetals 55*, T. Suski and W. Paul, Editors. 1998, Academic Press: San Diego. p. 117.
48. Wasmer, K., T. Wermelinger, A. Bidiville, R. Spolenak, and J. Michler, *In situ compression tests on micron-sized silicon pillars by Raman microscopy—Stress measurements and deformation analysis.* J. Mater. Res., 2008. **23**: p. 3040.
49. Ghisleni, R., J. Liu, R. Raghavan, P. Brodard, and J. Michler, *In-situ micro-Raman compression: Characterization of plasticity and fracture in GaAs.* Philosophical Magazine a-Physics of Condensed Matter Structure Defects and Mechanical Properties, 2009: p. in preparation.
50. Webster, S., D.N. Batchelder, and D.A. Smith, *Submicron resolution measurement of stress in silicon by near-field Raman spectroscopy.* Appl. Phys. Lett., 1998. **72**: p. 1478.
51. Wessel, J., *Surface-enhanced optical microscopy.* J. Opt. Soc. Am. B, 1985. **2**: p. 1538.
52. Fleischmann, M., P.J. Hendra, and A.J. McQuillan, *Raman spectra of pyridine adsorbed at a silver electrode.* Chem. Phys. Lett., 1974. **26**: p. 163.
53. Albrecht, M.G. and J.A. Creighton, *Anomalously Intense Raman Spectra of Pyridine at a Silver Electrode.* J. Am. Chem. Soc., 1977. **99**: p. 5215.
54. Jeanmaire, D.L. and R.P. Van Duyne, *Surface raman spectroelectrochemistry: Part I. Heterocyclic, aromatic, and aliphatic amines adsorbed on the anodized silver electrode.* Journal of Electroanalytical Chemistry, 1977. **84**: p. 1.
55. Michler, J., Y. Von Kaenel, J. Stiegler, and E. Blank, *Complementary application of electron microscopy and micro-Raman spectroscopy for microstructure, stress, and bonding defect investigation of heteroepitaxial chemical vapor deposited diamond films.* J. Appl. Phys., 1998. **83**: p. 187.
56. Anderson, M.S., *Locally enhanced Raman spectroscopy with an atomic force microscope.* Appl. Phys. Lett., 2000. **76**: p. 3130.
57. Pettinger, B., G. Picardi, R. Schuster, and G. Ertl, *Surface Enhanced Raman Spectroscopy: Towards Single Molecule Spectroscopy.* Electrochemistry, 2000. **68**(12): p. 942.
58. Stöckle, R.M., Y.D. Suh, V. Deckert, and R. Zenobi, *Nanoscale chemical analysis by tip-enhanced Raman spectroscopy.* Chem. Phys. Lett., 2000. **318**: p. 131.
59. Becker, M., et al., *The SERS and TERS Effects Obtained by Gold Droplets on Top of Si Nanowires.* Nano Lett., 2007. **7**(1): p. 75.
60. Becker, M., V. Sivakov, U. Gösele, T. Stelzner, G. Andrä, H.J. Reich, S. Hoffmann, J. Michler, and S.H. Christiansen, *Nanowires Enabling Signal-Enhanced Nanoscale Raman Spectroscopy.* Small, 2008. **4**(4): p. 398.
61. Christiansen, S.H., M. Becker, S. Fahlbusch, J. Michler, V. Sivakov, G. Andrä, and R. Geiger, *Signal enhancement in nano-Raman spectroscopy by gold caps on silicon nanowires obtained by vapour–liquid–solid growth.* Nanotechnology, 2007. **18**: p. 035503.

62. Maass, R., S. Van Petegem, D. Grolimund, H. Van Swygenhoven, D. Kiener, and G. Dehm, *Crystal rotation in Cu single crystal micropillars: In situ Laue and electron backscatter diffraction.* Applied Physics Letters, 2008. **92**(7): p. 071905.
63. Maass, R., S. Van Petegem, H. Van Swygenhoven, P.M. Derlet, C.A. Volkert, and D. Grolimund, *Time-resolved laue diffraction of deforming micropillars.* Physical Review Letters, 2007. **99**(14): p. 145505.
64. Wermelinger, T., C. Borgia, C. Solenthaler, and R. Spolenak, *3-D Raman spectroscopy measurements of the symmetry of residual stress fields in plastically deformed sapphire crystals.* Acta Mater., 2007. **55**: p. 4657.
65. Wermelinger, T. and R. Spolenak, *Correlating Raman peak shifts with phase transformation and defect densities: a comprehensive TEM and Raman study on silicon.* J. Raman Spectrosc., 2009. **40**: p. 679.
66. Yan, H.F., O. Kalenci, I.C. Noyan, and J. Maser, *Coherency effects in nanobeam x-ray diffraction analysis.* Journal of Applied Physics, 2008. **104**(2): p. 023506.

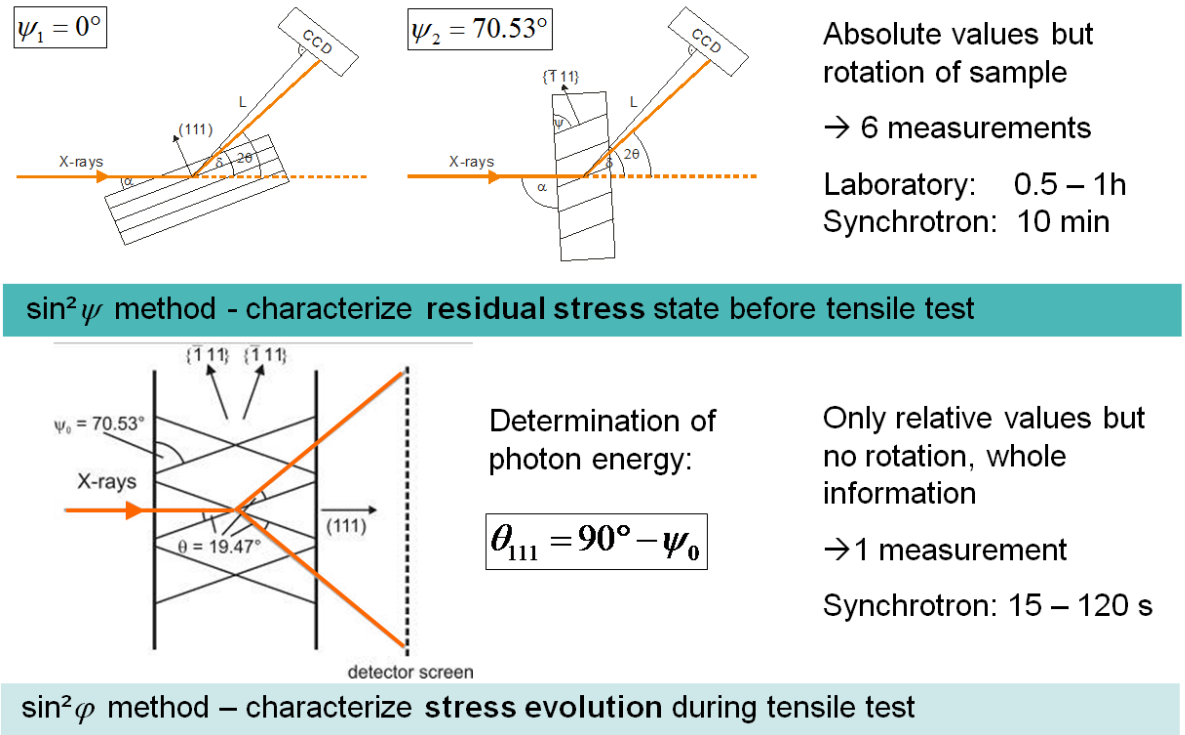

Figure 1. Comparison of diffraction geometries of the $\sin^2\psi$ – technique and the $\sin^2\varphi$ – technique. The (111) reflection is chosen for fcc metal thin films as the X-ray intensity needed to be maximized. For higher accuracy in strain higher order peaks are usually advisable.

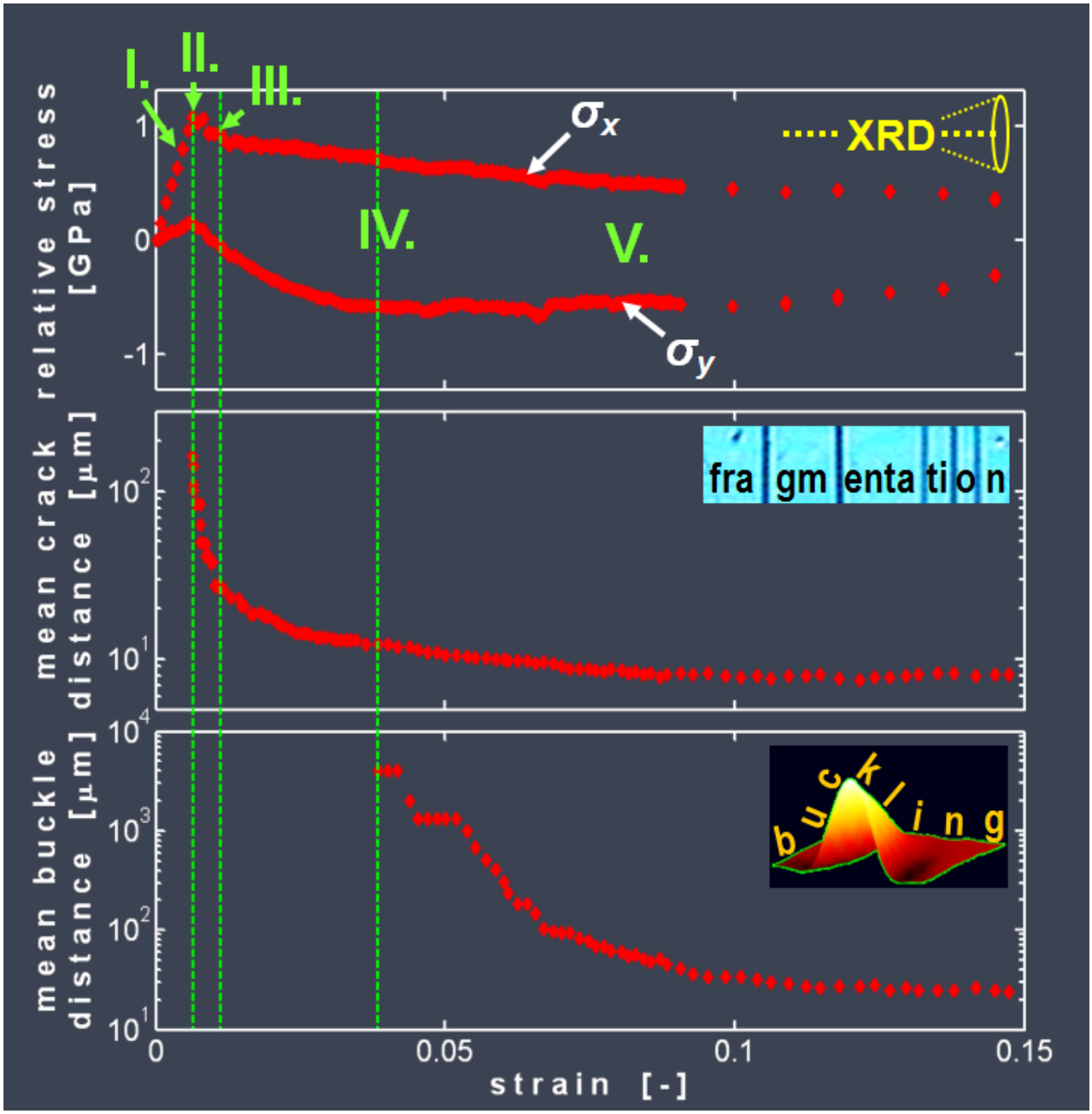

Figure 2. Fracture and delamination behavior of a 100 nm Ta film on a 125 mm polyimide substrate investigated by X-ray diffraction (without residual stress), optical microscopy and AFM. The different phases of deformation are the elastic regime (I), the onset of cracking (II), the steady-state cracking regime (III), the onset of delamination (IV) and the regime of predominant substrate deformation (V).

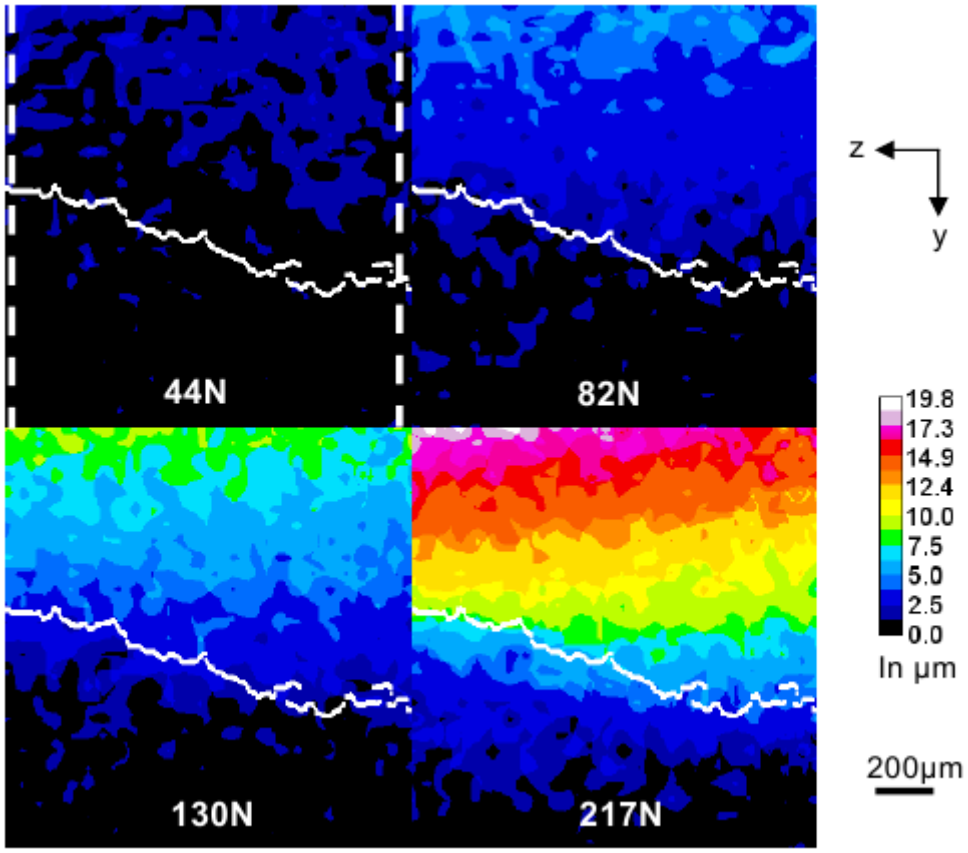

Figure 3. 2D map of the opening of a crack (mode I opening) in the interior of a cast iron sample obtained by DVC of tomographic images. The load is applied along the X axis (normal to the figure). The white line indicates the crack front (cracked surface above the line). For an applied load of 44N large black areas behind the crack tip (i.e. above the white line on the figure) indicates crack closure. When the load is increased, the crack gradually opens (adapted from ref. [35]).

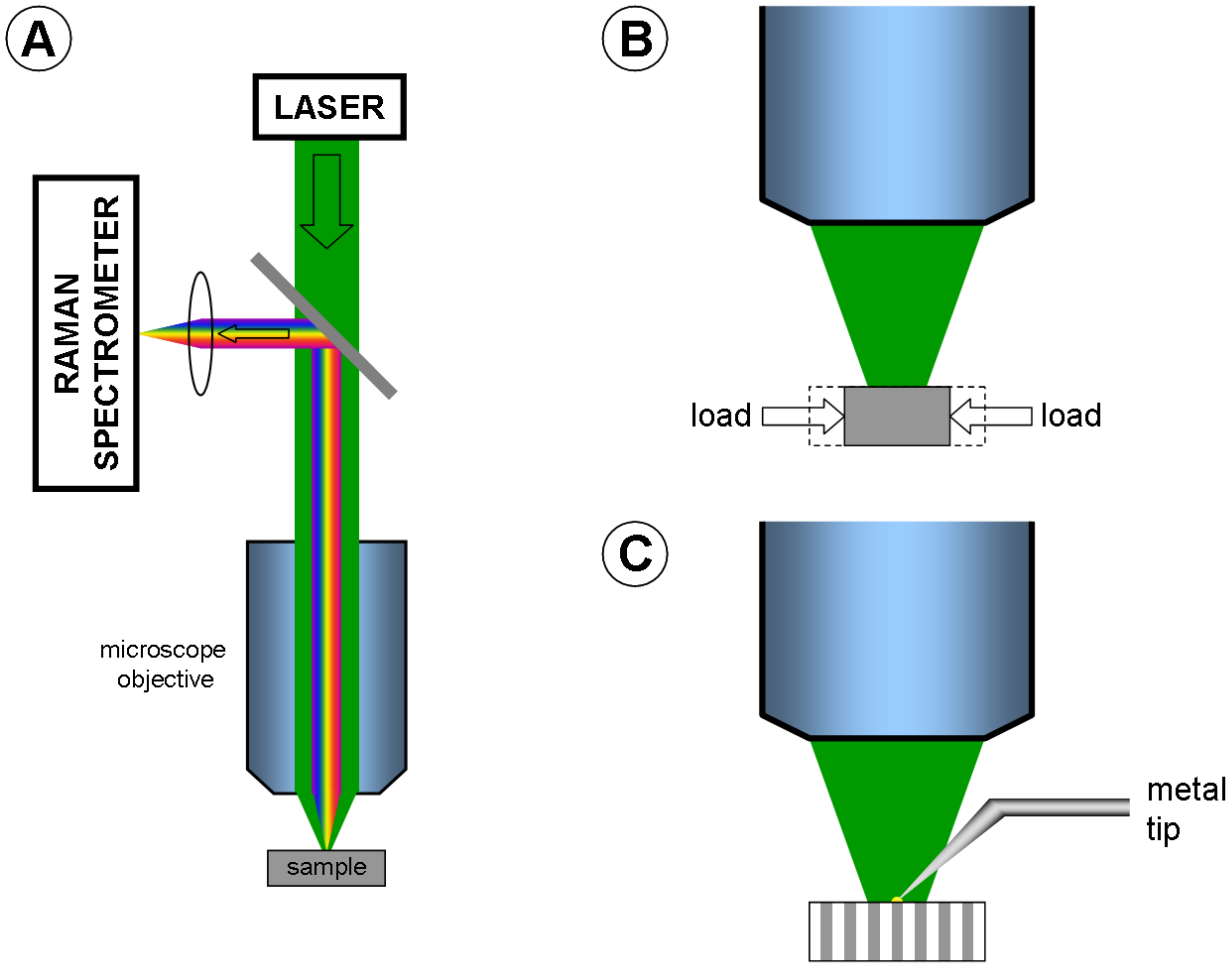

Figure 4. a) Principle of Raman spectroscopy: the laser is focused onto the sample for excitation (diffraction-limited spot ~ 1 μm), then the scattered light is collected through the same objective and dispersed into a spectrum by the spectrometer. b) in-situ μ-Raman for dynamic stress sensing: spectra are collected simultaneously during compression. c) TERS for nanoscale residual stress analysis: the metal tip localizes the excitation beyond the diffraction limit.